Inorganic Chemistry

Article

pubs.acs.org/IC

Terms of Use

A Well-Defined Terminal Vanadium(III) Oxo Complex

Amanda E. King,[†,‡,§] Michael Nippe,[†,‡,§] Mihail Atanasov,*[,∥,⊥] Teera Chantarojsiri,[†] Curtis A. Wray,[†] Eckhard Bill,[∥] Frank Neese,*[,∥] Jeffrey R. Long,*[,†,¶] and Christopher J. Chang*[,†,‡,▽,#]

[†]Department of Chemistry, University of California, Berkeley, California 94720-1460, United States

[‡]Chemical Sciences Division and [¶]Materials Sciences DivisionLawrence Berkeley National Laboratory, 1 Cyclotron Road, Berkeley, California 94720, United States

[▽]Department of Molecular and Cell Biology, University of California, Berkeley, California 94720-3200, United States

[#]Howard Hughes Medical Institute, University of California, Berkeley, California 94720, United States

[∥]Max-Planck Institut für Chemische Energiekonversion, Mülheim an der Ruhr D-45470, Germany

[⊥]Institute of General and Inorganic Chemistry, Bulgarian Academy of Sciences, Acad. Georgi Bontchev Str 11, 1113 Sofia, Bulgaria

Supporting Information

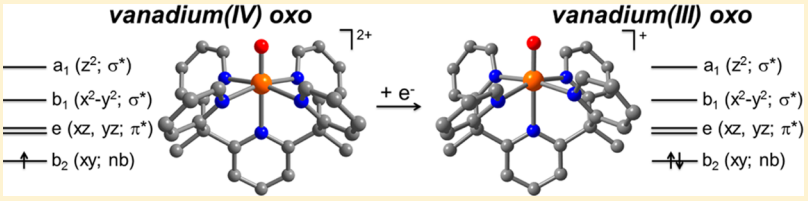

ABSTRACT: The ubiquity of vanadium oxo complexes in the V+ and IV+ oxidation states has contributed to a comprehensive understanding of their electronic structure and reactivity. However, despite being predicted to be stable by ligand-field theory, the isolation and characterization of a well-defined terminal mononuclear vanadium(III) oxo complex has remained elusive. We present the synthesis and characterization of a unique terminal mononuclear vanadium(III) oxo species supported by the pentadentate polypyridyl ligand 2,6-bis[1,1-bis(2-pyridyl)ethyl]pyridine ($PY5Me_2$). Exposure of $[V^{II}(NCCH_3)(PY5Me_2)]^{2+}$ (**1**) to either dioxygen or selected O-atom-transfer reagents yields $[V^{IV}(O)(PY5Me_2)]^{2+}$ (**2**). The metal-centered one-electron reduction of this vanadium(IV) oxo complex furnishes a stable, diamagnetic $[V^{III}(O)(PY5Me_2)]^{+}$ (**3**) species. The vanadium(III) oxo species is unreactive toward H- and O-atom transfer but readily reacts with protons to form a putative vanadium hydroxo complex. Computational results predict that further one-electron reduction of the vanadium(III) oxo species will result in ligand-based reduction, even though pyridine is generally considered to be a poor π-accepting ligand. These results have implications for future efforts toward low-valent vanadyl chemistry, particularly with regard to the isolation and study of formal vanadium(II) oxo species.

INTRODUCTION

Vanadium oxo complexes represent one of the most ubiquitous classes of metal oxo functionalities and have found diverse and widespread utilization in fields ranging from bioinorganic chemistry to heterogeneous and homogeneous catalysis. Our mechanistic understanding of vanadium haloperoxidases has relied heavily on spectroscopic and structural studies of the imidazolium-coordinated vanadate active site.[1] Vanadium oxo complexes also have demonstrated efficient catalytic oxidase reactivities in a diverse array of transformations (Scheme 1, left), including olefin epoxidations,[2] aromatizations of α,β-unsaturated cyclohexanone derivatives,[3] alcohol oxidations,[4] C−C bond cleavages of glycols to the corresponding ketones,[5] naphthol couplings,[6] and α-oxidation of hydroxyl esters and amides.[7] Hanson and co-workers have recently reported both the application and mechanism of vanadium-catalyzed oxidative degradation of lignin model complexes,[5] and the employment of appropriate ligand scaffolds has been shown to facilitate stereoselective couplings and catalytic resolutions of racemic mixtures of alcohols.[8] In contrast to the oxidative reactions listed above, Son and Toste recently disclosed a formally nonoxidative C−O bond cleavage employing a $V^{V}(O)$ catalyst supported by a tridentate Schiff base ligand.[9] In terms of reductive chemistry, Anson and co-workers have established that vanadium oxo complexes are key intermediates in electrocatalytic dioxygen reduction systems based on vanadium salen platforms.[10]

As a result of the universality and stability of vanadium oxo species, the electronic structures of vanadyl complexes of vanadium(IV) and (V) have been studied in detail and can be understood in terms of ligand-field theory, as outlined in a classic study by Ballhausen and Gray.[11] Scheme 1 (right) shows the expected molecular orbital (MO) diagram for the d^1 vanadyl species ($[V^{IV}(O)]^{2+}$) in a C_{4v}-symmetric ligand framework. On the basis of this simplified MO diagram, one-

Received: May 5, 2014
Published: August 6, 2014

 © 2014 American Chemical Society dx.doi.org/10.1021/ic5010177 | Inorg. Chem. 2014, 53, 11388−11395

Scheme 1. Diverse Oxidative Reactivity of Vanadium Oxo Complexes (left) and Energy-Level Diagram for the 3d Orbitals of a Representative C_{4v}-Symmetric Vanadium(IV) Oxo (Vanadyl) Species of Vanadium(IV) (right)

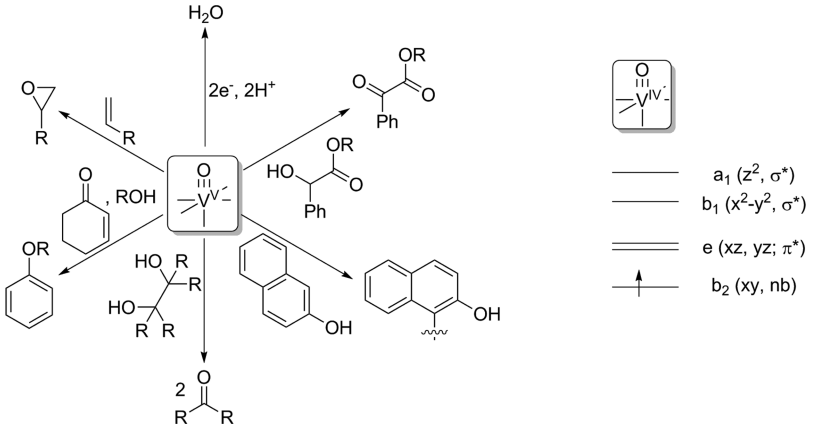

Scheme 2. Synthesis and Molecular Structures of the Cationic Complexes in 1−3[a]

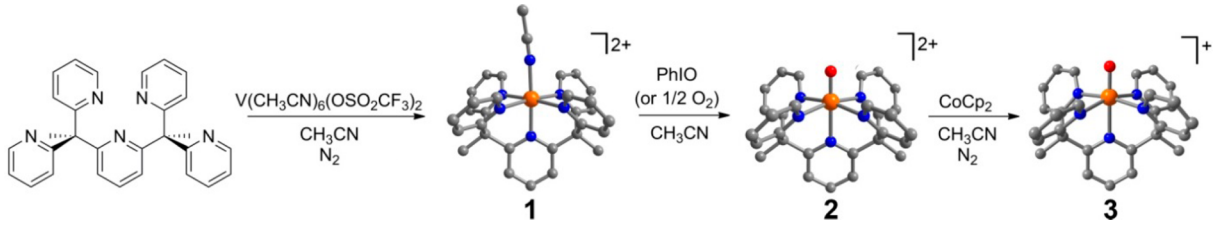

[a]Orange, blue, gray, and red spheres represent V, N, C, and O atoms, respectively; H atoms have been omitted for clarity.

Table 1. Comparison of Experimental and Computational B3LYP Bond Distances (Å) for Compounds 1−5 in the Most Stable Electronic/Geometric Configuration and Computational V−N Bond Lengths for the Series $[V(py)_6]^{4+/3+/2+/0}$ [a]

	1		2		3		4	5
	XRD	DFT, $S = {}^3/_2$	XRD[c]	DFT, $S = {}^1/_2$	XRD	DFT, $S = 0$	DFT, $S = {}^1/_2$	DFT, $S = 1$
$V-N_{CH_3CN}/V-O$	2.116(3)	2.144	1.595[2]	1.578	1.621(4)	1.598	1.614	1.825
$V-N_{py}$(ax)	2.096(2)	2.129	2.228[2]	2.296	2.266(5)	2.337	2.238	2.187
$V-N_{py}$(eq)[b]	2.116[2]	2.178	2.122[2]	2.146	2.094[5]	2.124	2.109	2.158
	$[V(py)_6]^{4+}$		$[V(py)_6]^{3+}$		$[V(py)_6]^{2+}$		$V(py)_6$	
	DFT, $S = {}^1/_2$		DFT, $S = 1$		DFT, $S = {}^3/_2$		DFT, $S = {}^1/_2$	
$V-N_{py}$(avg)	2.155		2.200		2.300		2.248	

[a]For a more complete listing of computed bond distances, see the SI. [b]Average of the four equatorial distances. [c]The structure contains two nonequivalent vanadium polyhedra in the unit cell.

electron reduction of the $[V^{IV}(O)]^{2+}$ core is expected to populate the nonbonding V d_{xy} orbital, yielding a low-spin ($S = 0$) vanadium(III) oxo system with unaltered V−O bond multiplicity. However, to the best of our knowledge, the isolation and characterization of a discrete terminal mononuclear vanadium(III) oxo species has not been reported. Indeed, the $[V(O)]^{+}$ species has been implicated in catalytic systems reported by Son and Toste,[9] Barhate and Chen,[6] and Hanson and co-workers,[5a] but the involvement of such species has relied either on indirect electron paramagnetic resonance (EPR) spectroscopic data or on the isolation of dinuclear $[V^{III}_2(O)]^{4+}$ cores. In this work, we present the synthesis, isolation, spectroscopic characterization, and computational investigation of six-coordinate $[V^{IV}(O)]^{2+}$ and $[V^{III}(O)]^{+}$ species supported by a pentapyridine ligand scaffold and examine their reactivity toward O- and H-atom-transfer (OAT and HAT) reactions and protonation. We also present data concerning both the accessibility and electronic structure of a hypothetical "$[V^{II}(O)]$" species.

RESULTS AND DISCUSSION

Synthesis and Characterization. Building on previous work from our laboratory on the development of robust coordination complexes supported by polypyridine ligands for hydrogen evolution catalysis[12] and dye-sensitized solar cell electron-transfer shuttles,[13] we reasoned that pentadentate platforms would allow for the isolation and characterization of unique vanadyl species with approximate C_{4v} symmetry. Complexation of the 2,6-bis[1,1-bis(2-pyridyl)ethyl]pyridine ($PY5Me_2$) ligand with $V^{II}(NCCH_3)_6(OTf)_2$ ($^{-}OTf = {}^{-}OSO_2CF_3$) in acetonitrile yields a dark-red, air-sensitive compound identified by X-ray crystallography as $[V^{II}(NCCH_3)(PY5Me_2)](OTf)_2$ (**1**; Scheme 2).[14] The V−N bond lengths are consistent with a high-spin electron configuration; this formulation is supported by B3LYP density functional theory

dx.doi.org/10.1021/ic5010177 | Inorg. Chem. 2014, 53, 11388−11395

(DFT) calculations, which favor the $S = {}^3/_2$ state over the $S = {}^1/_2$ state by 17.3 kcal/mol. The calculated V−N_{py}(eq), V−N_{py}(ax), and V−N_{CH_3CN} bond lengths compare reasonably well with the experimentally determined values of 2.116[3], 2.096[2], and 2.116(3) Å, respectively (Table 1). The UV−visible spectrum of **1** displays two transitions centered at 410 and 490 nm (Figure S1 in the Supporting Information, SI). Cyclic voltammetry studies reveal an irreversible oxidative redox event at 200 mV vs Fc/Fc^+ (Fc = ferrocene), which is assigned to the $V^{II/III}$ redox couple, and three irreversible reductive events at −2100, −2400, and −2650 mV vs Fc/Fc^+ (Figure S2 in the SI).

Exposure of acetonitrile solutions of **1** either to 1 equivalent of iodosobenzene or to a dioxygen atmosphere results in the formation of the vanadyl complex $[V^{IV}(O)(PY5Me_2)](OTf)_2$ (**2**; Scheme 2). Slow diffusion of diethyl ether into acetonitrile solutions of **2** produces single crystals suitable for X-ray diffraction (XRD) studies (Scheme 2). The average V−N_{py}(eq) bond lengths slightly elongate to 2.122[2] Å, while the V−N_{py}(ax) bond distance increases to 2.228[2] Å (Table 1). The newly installed V−O bond measures 1.595[2] Å and establishes **2** as a bona fide vanadium(IV) oxo species. As such, **2** exhibits the characteristic spectroscopic signatures of a $[V^{IV}(O)]^{2+}$ complex. The IR spectra of **2** and its ^{18}O-isotopomer reveal V−O stretches at 980 and 943 cm^{-1}, respectively (Figure S3 in the SI). The UV−visible spectrum displays a broad, weak band centered at 750 nm that presumably encompasses the $^2B_2 \rightarrow {}^2E$ transition; this assignment is supported by computations (773 nm; Table S2 in the SI; CASSCF). The $^2B_2 \rightarrow {}^2B_1$ transition is dipole-forbidden in the C_{4v} point symmetry but can gain vibronic intensity; charge-transfer bands become apparent at wavelengths of less than 400 nm (Figure S4 in the SI). The EPR spectrum of **2** displays the expected eight-line hyperfine splitting because of the $I = {}^7/_2$ ^{51}V (99.75% natural abundance) nucleus (Figure 1).

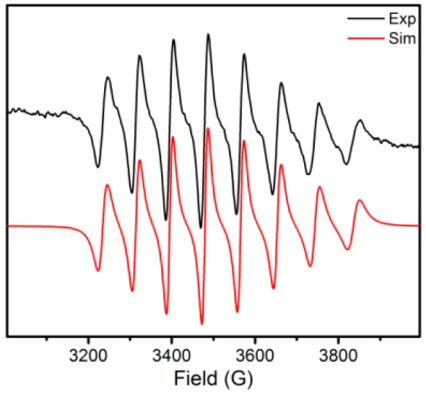

Figure 1. Room temperature X-band EPR spectrum of **2** in 99:1 CH_2Cl_2/CH_3CN (black, top) and simulated spectrum [g = 1.9745, $A(V^{51}, I={}^7/_2)$ = 79.2 × 10^{-4} cm^{-1}] (red, bottom).

The cyclic voltammogram of **2** displays a reversible redox event at −1220 mV vs Fc/Fc^+, indicating little structural rearrangement of **2** upon reduction and suggesting access to a formal vanadium(III) oxo species (Figure 2) because the free ligand does not exhibit redox chemistry in this potential window. Reaction of **2** with a slight stoichiometric excess of cobaltocene results in the formation of a dark-blue species identified as $[V^{III}(O)(PY5Me_2)]OTf$ (**3**) on the basis of X-ray

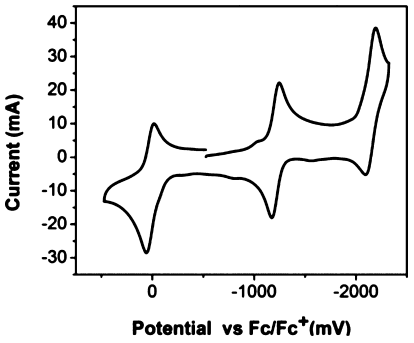

Figure 2. Cyclic voltammogram of **2**. Conditions: [**2**] = 1 mM, $[NBu_4PF_6]$ = 100 mM, acetonitrile solvent, scan rate = 100 mV/s, and working/reference/auxiliary electrodes = glassy carbon/silver wire/platinum wire. The Fc/Fc^+ couple is shown at 0 mV.

crystallography (Scheme 2). Upon reduction, the V−N_{py}(eq) bond lengths decrease to 2.094[5] Å, while the V−N_{axial} bond length increases to 2.266(5) Å. The V(O) functionality remains intact, with a significant increase in the V−O bond length to 1.621[4] Å, making it one of the longest reported terminal V−O bonds to date.[15]

The IR spectra of **3** and its ^{18}O-isotopomer reveal stretches at 929 and 895 cm^{-1}, respectively (Figure S5 in the SI). Notably, the shift in energy observed on going from **2** to **3** agrees with the increase in the V−O bond length observed upon reduction. The UV−visible−near-IR (NIR) spectrum of **3** shows transitions at 1065, 710, and 600 nm and a shoulder at 495 nm (Figure S6 in the SI). Compound **3** is diamagnetic, as evidenced by its solution ^1H NMR spectrum (see the Experimental Section).

Attempts to extend the crystallographic series to include putative oxidized "V^V" or reduced "V^{II}" species were unsuccessful. No reaction was observed when **2** was exposed to strong oxidants such as NO^+, and efforts to metalate $PY5Me_2$ with vanadium(V) oxo starting materials resulted in the isolation of **2**. These observations suggest that a $PY5Me_2$-ligated $[V^V(O)]^{3+}$ complex would be a powerful oxidant. Such oxidative behavior could be attributed to the $PY5Me_2$ ligand potentially being π-accepting from the d_{xy} orbital. Furthermore, the electrochemical results shown in Figure 2 suggest that the one-electron reduction of **3** is chemically reversible on the time scale of the cyclic voltammetry experiment. However, repeated attempts to isolate the neutral $[V^{II}(O)PY5Me_2]$ (**4**) species have been unsuccessful to date. As discussed in the following, we utilized DFT and ab initio computational studies to interrogate the electronic structure of this unprecedented, highly reduced metal oxo entity.

Computational Studies. The crystallization of **2** and **3** offers a unique opportunity to examine the electronic structure of a terminal $[V^{III}(O)]^+$ and compare it with that of the $[V^{IV}(O)]^{2+}$ moiety in an identical ligand environment. The V−ligand atom distances obtained from DFT geometry optimizations for **2** and **3** utilizing the B3LYP functional (and BP86; see the SI) agree well with the crystallographically determined bond lengths (Table 1), with agreement between the experimental and theoretical V−O and V−N_{eq} bond distances in favor of BP86 compared to B3LYP (Tables S9 and S10 in the SI). However, V−N bond distances trans to V−O are overestimated by 0.041−0.071 Å in both methods.

For complex **2**, Löwdin spin-population analysis from DFT (B3LYP; Table 2) and CASSCF (Table S8 in the SI) and spin-

dx.doi.org/10.1021/ic5010177 | Inorg. Chem. 2014, 53, 11388−11395

Table 2. Löwdin Spin Populations (Q) from DFT (B3LYP) and V−Ligand Bonding[a] As Revealed by Ligand-Field Angular Overlap Analysis of CASSCF Electronic Wave Functions from NEVPT2 Multireference Electronic Structure Calculations for Compounds 1−5 and the Model Compound Series $[V(py)_6]^{4+/3+/2+/0}$

	1	2	3	4	5
Q(V)	2.72	1.10		−0.51	1.949
Q(O,N)	−0.05	−0.14		0.09	−0.016
$Q(C,H,N)_{py}$	0.33	0.04		1.42	0.009
$e_\sigma(O)$		29440	22168		
$e_\pi(O)$		18672	13718		
$e_\sigma(N_{py})$		9116	9293		
$e_{\pi s}(N_{py})$		856	2003		
	$[V(py)_6]^{4+}$	$[V(py)_6]^{3+}$	$[V(py)_6]^{2+}$	$[V(py)_6]$	
Q(V)	1.18	2.02	2.89	2.66	
Q(N)	−0.12	−0.08	−0.06	−0.49	
Q(C,H)	−0.06	0.06	0.17	−1.17	
$e_\sigma(N)$	10466	6061	2682		
$e_{\pi s}(N)$	3292	828	−1706		

[a]Positive (negative) values of angular overlap model parameters reflect antibonding (bonding) interactions.

density plots (Figure 3) show that the single spin ($S = {}^1/_2$) resides in a nonbonding MO localized on vanadium (d_{xy},

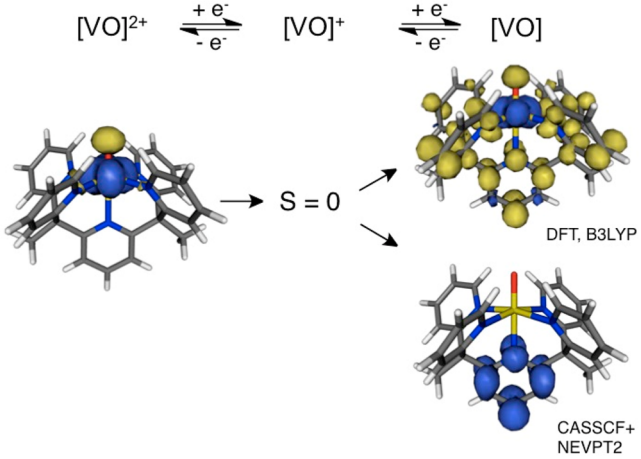

Figure 3. Ground-state spin-density plots from DFT (B3LYP) for **2** (left) and the two computational $S = {}^1/_2$ ground-state solutions for the hypothetical complex **4** of conjectured formal valence structure "$[V^{II}(O)]$" (right) according to DFT [V^{IV} open-shell biradical ($S = 1$) ligand] and CASSCF + NEVPT2 (V^{III} single-radical ligand). Löwdin spin populations Q at V and O atoms and the total of the N, C, and H atoms are listed in Table 2 (DFT and B3LYP) and Table S8 in the SI(CASSCF).

91.5%, B3LYP, quasi-restricted orbitals). Computed spectroscopic parameters of $g = 1.978$ and $A = -79.62\times 10^{-4}$ cm^{-1} agree nicely with the experimentally determined values of $g = 1.9745$ and $A = 79.2 \times 10^{-4}$ cm^{-1} when using a PBE0 hybrid functional.[16] Acceptable but less satisfactory values are given by the B3LYP functional ($g = 1.979$ and $A = 66.02.10^{-4}$ cm^{-1}). An analysis of A in terms of Fermi contact, spin-dipolar, and spin−orbit coupling energies show that the latter yield only 6% to the total A (Table S11 in the SI).

The results from CASSCF and NEVPT2 indicate that the $^2B_2(d_{xy})$ ground state for **2** is followed by $^2E(d_{xz},d_{yz})$, $^2B_1(d_{x^2-y^2})$, and $^2A_1(d_{z^2})$ excited states (Table S2 in the SI). The strong V−O σ- and π-antibonding interactions place the d_{z^2} and (d_{xz}, d_{yz}) orbitals high in energy, and V−N_{py} σ-donor interactions destabilize *both* the d_{z^2}(axial pyridine) and $d_{x^2-y^2}$ orbitals.

On the basis of the simplified MO diagram shown in Scheme 1, a $[V^{III}(O)]^+$ species would be expected to adopt a low-spin ($S = 0$) ground state upon the addition of an electron to the half-occupied nonbonding d_{xy} orbital found in **2**. This electronic structure implies an isoelectronic relationship between **3** and previously reported chromium(IV) oxo,[17] manganese(V) oxo[18] and nitrido,[19] and iron(VI) nitrido[20] species in tetrapodal ligand fields. In accordance with the diamagnetic ^{1}H NMR solution spectrum of **3** at room temperature, the $S = 0$ ground state of **3** is consistently favored by both DFT (5.26 and 7.66 kcal/mol for B3LYP and BP86; Table S3 in the SI) and CASSCF/NEVPT2 (5.91 kcal/mol; Table S8 in the SI) computations. As in **2**, the electron density is largely located on the vanadium-based d_{xy} orbital but with some spin density delocalized on the π^* orbitals of the axial pyridine fragment (Figure S7 in the SI). Compound **3** adopts a singlet ground state mostly because of the large splitting between the d_{xy} and (d_{xz}, d_{yz}) orbitals that is caused by strong π interactions of the vanadium-based d_{xz} and d_{yz} orbitals with both the π orbitals of the oxo and $PY5Me_2$ pyridine ligands. The experimentally observed decrease in the ν(V−O) stretching frequency of 50 cm^{-1} on going from **2** to **3** is reasonably well reproduced computationally (~30 cm^{-1}; Figures S8 and S9 in the SI).

Given the classical orbital considerations discussed above, one-electron reduction of **3** to yield **4** would be expected to furnish a $[V^{II}(O)]$ species with a single unpaired electron in degenerate d_{xz}/d_{yz} orbitals ($S = {}^1/_2$), thereby lowering the formal V−O bond order to 2.5. Interestingly, we find that this configuration is not the case. While both DFT (B3LYP, Table 1; BP86, Tables 1 and S5 in the SI) and CASSCF/NEVPT2 (Table S8 in the SI) calculations predict **4** to have a doublet ground state (see also Figure S10 in the SI), the oxidation state of vanadium cannot be described as +II. Instead, it is predicted that V−O bonding interactions are stabilized by V−N_{py} π interactions, which allow for charge transfer, corresponding to one (CASSCF) or two (DFT/B3LYP) electrons from vanadium to the pyridine π^* system of the ligand. As such, DFT/B3LYP predicts [$(PY5Me_2)V(O)$] to contain a V^{IV} ion (d_{xy}^1) antiferromagnetically coupled to an open-shell ($S = 1$) biradical ligand, while the CASSCF/NEVPT2 results favor a formulation corresponding to a V^{III} ion (d_{xy}^2) and a single spin contained within π^* orbitals of the axial pyridine (CASSCF/NEVPT2) moiety (Figure 3). These computational findings suggest that the V^{III} ion in **3** is in the lowest possible metal oxidation state for the $PY5Me_2$ V−O series.

Even though pyridines are commonly considered poor π acceptors, it is obvious from the foregoing discussion that V−py π interactions can be significant and lead to charge transfer to prevent the formation of a $[V^{II}(O)]$ species. In order to analyze these interactions further, we also studied the chemical bonding in the homoleptic series of complexes $[V(py)_6]^q$ (q = 4+, 3+, 2+, and 0; Figure S11 and Table S6 in the SI); V−N bond distances and Löwdin spin populations from B3LYP geometry optimizations for this series are listed in Tables 1 and 2. The species $[V^{IV}(py)_6]^{4+}$, $[V^{III}(py)_6]^{3+}$, and $[V^{II}(py)_6]^{2+}$ behave as Werner type complexes with $S = {}^1/_2$, 1, and ${}^3/_2$ ground states, respectively. Pyridine π donation results in π-antibonding

dx.doi.org/10.1021/ic5010177 | Inorg. Chem. 2014, 53, 11388−11395

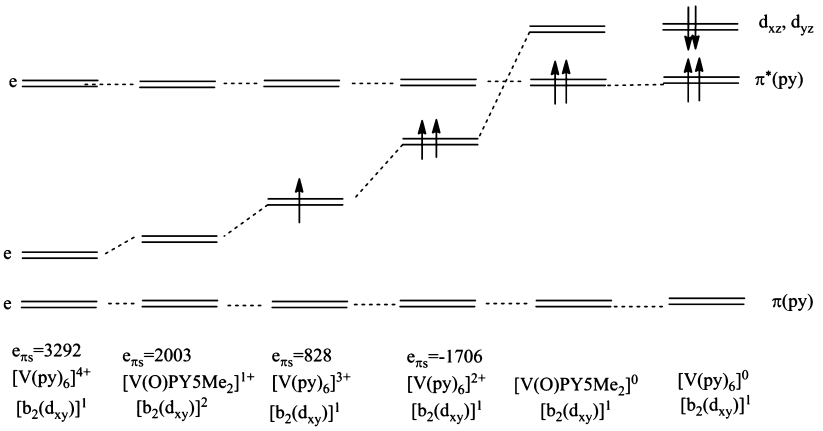

Figure 4. Comparison of the one-electron energy-level schemes (schematic, D_4 symmetry) from ligand-field analysis of NEVPT2/CASSCF energies and wave functions of complexes with well-defined metal-based oxidation states for $[V(O)PY5Me_2]^+$ (**3**) with their $[V(py)_6]^{n+}$ (n = 4, 3, 2) congeners. The $b_2(d_{xy})$ orbital is singly occupied for $[V^{IV}(py)_6]^{4+}$, $[V^{III}(py)_6]^{3+}$, $[V^{II}(py)_6]^{2+}$, $[V(O)PY5Me_2]^0$, and $[V(py)_6]^0$ and doubly occupied in the ground state of **3** [while not shown, the $b_2(d_{xy})$ occupancy was indicated for each plot]. Orbital energy diagrams for complexes $[V(O)PY5Me_2]^+$ and $[V(py)_6]^0$ with DFT B3LYP metal-radical ground-state formulations are represented schematically on the right side of the diagram.

interactions ($e_{\pi s}$) for $[V^{IV}(py)_6]^{4+}$ (d_{xy}^1), which decrease upon reduction in $[V^{III}(py)_6]^{3+}$ (d_{xy}^1, $d_{xz,yz}^1$), and become bonding for $[V^{II}(py)_6]^{2+}$ (d_{xy}^1, d_{xz}^1, d_{yz}^1), in which the pyridine ligands now act as π acceptors (Table 2). In contrast, the presence of the strong oxo ligand in **2** and **3** causes an increase of V−py π-antibonding interactions on going from $[V^{IV}(O)]^{2+}$ (d_{xy}^1) in **2** to $[V^{III}(O)]^+$ (d_{xy}^2) in **3**. Interestingly, a ground-state charge transfer from V to ligand π^* orbitals, similar to the one proposed for **4**, is also apparent for $[V(py)_6]$. Because the e(d_{xz},d_{yz}) metal orbitals become comparable in energy with the e(π^*) pyridine MOs, two electrons are transferred from V to py to form a high-spin vanadium(III) (d^3, S = $^3/_2$)−pyridine biradical (S = 1) pair (Table 2 and Figure 4). Antiferromagnetic coupling (like in the case of **4**) results in a doublet ground state of $[V(py)_6]$. However, while transfer of the electron density occurs from V σ-antibonding d_{z^2} and $d_{x^2-y^2}$ orbitals in the case of $[V(py)_6]$, π-type (d_{xz}, d_{yz}) orbitals are involved in **4**. Therefore, the driving force for charge-transfer ground states in the two complexes lies in the gain of energies of σ(V−N) (for $[V(py)_6]$) and π(V−O) (for **4**) bonding interactions and the lowering of kinetic energy due to the delocalization of two 3d electrons over the pyridine π^* network.

Reactivity Studies. The successful isolation of **2** and **3** allows for comparative reactivity studies of $[V^{III}(O)]^+$ and $[V^{IV}(O)]^{2+}$ species in HAT, OAT, and protonation reactions. The majority of previous studies examining the HAT reactivity of vanadium oxo complexes have focused on the reduction of $[V^V(O)]^{3+}$ species to yield $[V^{IV}(OH)]^{3+}$ hydroxo complexes; one example of self-exchange between $V^V(O)_2$ and $V^{IV}(O)$-(OH) has been reported.[21] The OAT ability of the $[V^{IV}(O)]^{2+}$ species has thus far only been reported to extend to V^{II} centers, leading to the formation of dinuclear V^{III}−O−V^{III} species. Another key characteristic of vanadyl functional groups is their stability toward acidic conditions. In this regard, compound **2** behaves like an archetypical $[V^{IV}(O)]^{2+}$ species. Accordingly, it was found to be unreactive toward O-atom acceptors such as triphenylphosphine, HAT reagents such as cyclohexadiene and dihydroanthracene, and strong acids.

Compound **3** also proved to be unreactive toward HAT reagents. No OAT reactivity was observed upon exposure of **3** to excess triphenylphosphine at 70 °C over 20 h, suggesting that **3** is best described as a nucleophilic metal oxo species. Indeed, the nucleophilic nature of **3** is further corroborated by the rapid reaction of electrochemically generated **3** with acids of varying strengths (Figure 5). The addition of acid triggers a rise

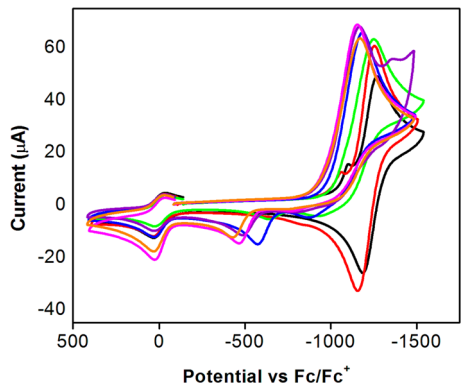

Figure 5. Cyclic voltammetry of **2** in acetonitrile under an anaerobic atmosphere in the presence of equimolar amounts of phenol (black), 2-bromophenol (red), acetic acid (green), benzoic acid (blue), 4-nitrobenzoic acid (purple), chloroacetic acid (pink), or cyanoacetic acid (orange). Ferrocene was added as an internal reference and is seen at $E_{1/2}$ = 0 mV. Conditions: [**2**] = 1 mM, [acid] = 1 mM, $[NBu_4PF_6]$ = 100 mM, scan rate = 100 mV/s, working/reference/auxiliary electrodes = glassy carbon/silver wire/platinum wire.

in the current at potentials positive of the $V^{IV/III}(O)$ reduction potential. As the acid strength increases, the reversibility of the $V^{IV/III}(O)$ redox couple is lost until an irreversible wave with a E_{pc} ∼ −510 mV vs Fc/Fc^+ appears. Comparison of the integrated cathodic peak areas obtained in the presence and absence of 1 equiv of acid relative to **2** reveals an approximate 2:1 electron/proton ratio, suggesting the electrochemical-chemical-electrochemical (ECE) process described in eq 1.

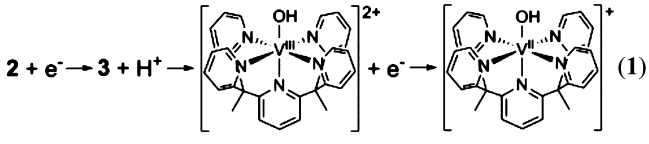

(1)

dx.doi.org/10.1021/ic5010177 | Inorg. Chem. 2014, 53, 11388−11395

Protonation of **3** to yield the transient $[V^{III}(OH)]^{2+}$ (**5**) species was further investigated by DFT calculations. As expected, the V−O bond elongates to 1.83 Å, indicative of a vanadium(III) hydroxo species (Tables 1 and 2). Protonation is predicted to cause a spin state change to $S = 1$ (Table S7 in the SI). Accordingly, the much weaker trans influence imparted by a hydroxo ligand compared to an oxo ligand causes the V−N_{py}(ax) bond distance to be shortened by ∼0.16 Å upon protonation of **3**. It is interesting to compare these results to the reported observations for the related molecular proton reduction catalyst $[(PY5Me_2)Mo^{IV}(O)]^{2+}$.[12a] In the latter case, it could be established that one-electron reduction and protonation of the $[Mo^{IV}(O)]^{2+}$ (d^2, $S = 0$) unit results in the formation of a $[Mo^{III}{=}(OH)]^{2+}$ (d^3, $S = {}^1/_2$) species that retains Mo=O multiply bonded character.[12d] The reactivity of **3** contrasts with that of the $[Mo^{IV/III}(O)]^{2+/+}$ species in this regard; while $[Mo^{III}{=}(OH)]^{2+}$ can be considered a protonated Mo-oxo species, the less diffuse valence d orbitals of V (compared to Mo) result in weaker M−O bonding interactions and render **5** a vanadium(III) hydroxo complex. This significant difference in the electronic structure of the reduced−protonated species may lead to a new mechanistic route for metal oxo catalyzed proton reduction reactions, a concept that is currently under investigation.

CONCLUDING REMARKS

Utilization of the pentapyridine ligand $PY5Me_2$ allowed for preparation of the corresponding vanadyl complex **2** featuring a $[V^{IV}(O)]^{2+}$ unit. One-electron reduction of **2** yields diamagnetic **3**, which constitutes the first example of an isolated monomeric $[V^{III}(O)]^{+}$ species. Compounds **2** and **3** are unreactive toward both OAT and HAT reagents, but **3** is reactive to protonation to generate vanadium hydroxide species. Interestingly, electrochemical data indicate that the neutral $[(PY5Me_2)V(O)]$ complex **4** could also be accessible, but computational results predict that **4** will not feature the anticipated d^3 $[V^{II}(O)]$ unit but rather that the transfer of one (CASSCF) or two (DFT) electrons from vanadium to the π^* system of the ligand is energetically favored. These results indicate that the $[V^{III}(O)]^{+}$ unit within **3** likely constitutes the lowest possible valence for vanadium within a vanadium oxo group stabilized by π-accepting ligands. The combined experimental and computational findings have implications for invoking low-valent vanadium oxo species in a diverse range of catalytic transformations.

EXPERIMENTAL SECTION

General Details. Unless otherwise stated, all manipulations were performed in a Vacuum Atmospheres model glovebox under an atmosphere of purified dinitrogen. Solvents were obtained anhydrous and oxygen-free from a Vacuum Atmospheres Solvent Purification System or by analogous methods. Celite, molecular sieves, and alumina were dried by heating at 200 °C under a dynamic vacuum for at least 24 h prior to use. All glassware was oven-dried at temperatures greater than 170 °C prior to use. The ligand $PY5Me_2$ and $V(NCCH_3)_6(OTf)_2$ were prepared according to literature procedures;[22] all other materials were purchased and used as received. UV−visible spectra were recorded on a Hewlet-Packard 8452A photodiode array spectrometer. IR spectra were acquired on a Bruker Alpha Fourier transform infrared specrophotometer using a diamond ATR accessory. Cyclic voltammetry experiments were carried out using BASI's Epsilon potentiostat. A glassy carbon working electrode and silver (reference) and platinum (auxiliary) wire electrodes were used for cyclic voltammetry experiments in acetonitrile with Bu_4NPF_6 as a supporting electrolyte. Ferrocene ($E_{Fc^+/0}$ = 0.64 V vs SHE) was added during each experiment as an internal reference. Carbon, hydrogen, and nitrogen elemental analyses were obtained from the Microanalytical Laboratory at the University of California, Berkeley. ^{1}H NMR spectra were obtained using an AVANCEIII 500 instrument. X-band EPR spectra of **2** were acquired using a Bruker ELEXSYS spectrometer.

Crystal Structure Determinations. Data collections were performed on single crystals coated with Paratone-N oil and mounted on Kaptan loops. The crystals were frozen under a stream of dinitrogen (100 K; Oxford Cryostream 700) during measurements. Data were collected using a Bruker APEX-II QUAZAR diffractometer equipped with a Microfocus Sealed Source (Incoatec ImS; Mo Kα, λ = 0.71073 Å) and an APEX-II detector (NIH Shared Instrumentation; Grant S10-RR027172). Raw data were integrated and corrected for Lorentz and polarization effects using Bruker *APEX2 v2009*.[23] Absorption corrections were applied using *SADABS*.[24] Space group assignments were determined by examination of systematic absences, *E* statistics, and successive refinement of the structures. Structures were solved using either the Patterson method (**1** and **3**) or direct methods (**2**) and refined by least-squares refinement on F^2 followed by difference Fourier synthesis.[25] All H atoms were included in the final structure factor calculation at idealized positions and were allowed to ride on the neighboring atoms with relative isotropic displacement coefficients. Thermal parameters were refined anisotropically for all non-H atoms. Data refinement was standard with the following exemptions: Both $^-OSO_2CF_3$ counterions in the structure of **1** are disordered over two positions with relative occupancies of 0.65/0.35 and 0.74/0.26. Similarly, the $^-OSO_2CF_3$ counterion in the structure of **3** shows disorder over two major orientations with 0.58/0.42 relative occupancies, with the S atom of the major orientation being disordered in itself.

Synthesis of $[V(PY5Me_2)(NCCH_3)](OTf)_2$ (1). A solution of $PY5Me_2$ (100 mg, 0.225 mmol, 1 equiv) in 2 mL of acetonitrile was combined with a solution of $[V(NCCH_3)_6](OTf)_2$ (134 mg, 0.225 mmol, 1 equiv) in 3 mL of acetonitrile. The resulting mixture was allowed to stir overnight, and the dark-red reaction mixture was concentrated to ∼2 mL; single crystals for XRD were obtained via Et_2O diffusion into this concentrated acetonitrile solution (157 mg, 0.178 mmol, 79%). The resulting crystals were dried extensively in vacuo prior to further analysis. Anal. Calcd for $C_{33}H_{28}F_6N_6O_6S_2V$ (**1**): C, 47.54; H, 3.39; N, 10.08. Found: C, 47.18; H, 3.01; N, 9.91.

Synthesis of $[V(O)(PY5Me_2)](OTf)_2$ (2). Two methods proved to be viable synthetic routes. In the first route, a dark-red solution of **1** (50.0 mg, 0.060 mmol) in 5 mL of MeCN was exposed to O_2 with stirring for 15 h. The light-green solution was concentrated and recrystallized via Et_2O diffusion (36.4 mg, 0.045 mmol, 75%). In the second route, a solution of $[V(PY5Me_2)(MeCN)](OTf)_2$ (100 mg, 0.120 mmol, 1 equiv) was exposed to PhIO (34.0 mg, 0.156 mmol, 1.3 equiv) in acetonitrile under a dinitrogen atmosphere. The initially dark-red solution changed to light green. Crystals suitable for XRD were grown via Et_2O diffusion into a concentrated MeCN solution of **2** (89.3 mg, 0.110 mmol, 92%). Anal. Calcd for $C_{34}H_{28.5}F_6N_{6.5}O_7S_2V$ (**2**·1.5CH_3CN): C, 46.93; H, 3.51; N, 10.46. Found: C, 47.39; H, 3.27; N, 10.49.

Synthesis of $[V(O)(PY5Me_2)](OTf)$ (3). A solution of **2** (100 mg, 0.123 mg, 1 equiv) was exposed to cobaltocene (30 mg, 0.160 mmol, 1.3 equiv) in 5 mL of MeCN under a dinitrogen atmosphere. The initial green solution immediately turned dark blue. After stirring overnight, the reaction mixture was dried in vacuo, and the resulting dark residue was titurated with tetrahydrofuran (THF; 20 mL) for 24 h. The suspension was filtered, and the dark-blue powder washed with a copious amount of THF until the filtrate ran clear. Crystals suitable for XRD were grown via Et_2O diffusion into a concentrated CH_2Cl_2 solution of **3** (72.0 mg, 0.109 mmol, 88%). Anal. Calcd for $C_{63}H_{56}Cl_6F_6N_{10}O_8S_2V_2$ (**3**·1.5CH_2Cl_2): C, 48.08; H, 3.59; N, 8.90. Found: C, 48.54; H, 3.32; N, 8.86. ^{1}H NMR (CD_3CN, 500 MHz, ppm): δ 9.43 (4H, d), 8.09 (1H, t), 7.90 (2H, d), 7.86 (4H, t), 7.66 (4H, t), 7.25 (4H, t), 2.79 (6H, s).

Computations and Ligand-Field Analysis. All calculations were carried out employing the *ORCA* program suite.[26] DFT geometry

dx.doi.org/10.1021/ic5010177 | *Inorg. Chem.* 2014, 53, 11388−11395

optimizations were performed using the B3LYP and BP86 exchange-correlation potentials and def2-TZVP ZORA basis sets. To speed up the B3LYP geometry optimizations, the resolution of identity (RI) "chain-of-spheres exchange (COSX)" (RICOSX) algorithm,[27] together with the split-RI-J procedure[28] (a density-fitting variant) for computation of the Coulomb matrix elements, was used along with a modest angular grid (default value Grid3). To ensure a reliable accuracy, optimized geometries and wave functions from these calculations were used as input in refined geometry optimizations, making use of larger angular grids for the numerical integration (Grid6 for RI and Gridx7 for RIJCOSX).

Geometry optimizations using the complete active-space self-consistent-field method (CASSCF)[29] were also performed. However, dynamical correlation, which is missing in the calculation of CASSCF energy gradients, resulted in geometries wherein equatorial V−N_{py} bond distances were largely overestimated (by as much as 0.15−0.20 Å). Starting with the DFT/B3LYP-optimized geometries CASSCF and following N-electron valence second-order perturbation theory (NEVPT2)[30] calculations were carried out by initially distributing n electrons on five orbitals that were assumed to be dominated by the V 3d functions (V^z, n = 1−3 for z = IV, III, and II, respectively). To this end, an initial guess for the electron density (starting with the default "PModel" guess) was adopted in a state average CASSCF(n,5) calculation, where for the complexes of V^{III} and V^{II} state averaging was performed over *both high- and low-spin* states. Such a procedure ensures better CASSCF convergence than that in state-specific calculations. The resulting state-averaged orbitals were then utilized in a second step in state-specific ground-state calculations. Inspection of the orbitals from state-average CASSCF calculations leads to the following observation: orbitals within the active space were dominated by V 3d functions for both the X-ray and B3LYP DFT-optimized geometries of complexes **2** (V^{IV} d^1) and **3** (V^{III} d^2). In marked contrast, for **3** (BP86-optimized geometry) and **4**, only three orbitals (out of the five orbitals in the active space) were dominated by the V 3d functions; the other two orbitals turned into the pyridine π^* type. Extensions of the active space with four more orbitals, the doubly occupied O $\pi(p_x, p_y)$ and the ligand counterparts of the $d_{x^2-y^2}$ and d_{z^2} orbitals for **2** and **3**, did not lead to changes either in the relative energies of the alternative spin ground states or in the spin distributions, as deduced from Löwdin spin populations. It follows from natural orbital populations that the ground states of all three complexes are to good approximations of the single-reference type. Taking, for example, the S = 1 ground state of **3**, the natural orbital occupation vector (2, 2, 2, 2, 0.987, 0.987, 0.013, 0.013, 0.000) from a CAS(2,5) calculation did not change when extending the active space to CAS(10,9) (2.000, 1.999, 1.999, 1.999, 0.987, 0.987, 0.013, 0.013, 0.000). These results justify the use of single-reference DFT for the considered complexes.

State-average CASSCF/NEVPT2 calculations showed well-defined d^1 (V^{IV}, **2**) and d^2 (V^{III}, **3**) type multiplets to afford a characterization of the metal−ligand V−O and V−N interactions using ligand-field analysis. To this end, we adopted the angular overlap model[31] and adjusted its parameters from a best fit to the 5 × 5 ligand-field matrices resulting from the ab initio calculations. To obtain these matrices, we applied our recently developed ab initio based ligand-field theory.[32] This allows all parameters of the general (nonadditive) ligand field to be obtained using a one-to-one mapping of matrix elements of the ligand-field Hamiltonian (which depends linearly on these parameters) on the CASSCF and NEVPT2 results. In the angular overlap parametrization of the ligand field, we assumed oxygen as a linear ligator represented by two energy parameters, e_σ(O) and e_π(O), describing V−O σ and π antibonding, respectively. The V−py interactions were accounted for by two parameters, $e_\sigma(N_{py})$ and $e_{\pi s}(N_{py})$. These parameters describe the V−N σ and out-of-plane π bonding, where π interactions between V and N orbitals within the pyridine plane were neglected ($e_\sigma(N_{py})$ = 0). The angular overlap matrices, depending linearly on these parameters, have been set up, making use of the angular geometries from the DFT-optimized structures. For **2** and **3**, the angular overlap parameters for the V−O and V−N bonds were compared with bonding parameters for the hypothetical analogous isoelectronic $[V(py)_6]^{4+}$ and $[V(py)_6]^{3+}$ model complexes.

■ ASSOCIATED CONTENT

Supporting Information

X-ray crystallographic data in CIF format, UV−visible spectra for **1** and **2**, UV−visible−NIR spectrum for **3**, IR spectra for **2** and **3**, cyclic voltammogram of **1**, and computational details for compounds **1**−**5**. This material is available free of charge via the Internet at http://pubs.acs.org.

■ AUTHOR INFORMATION

Corresponding Authors

*E-mail: mihail.atanasov@cec.mpg.de.
*E-mail: frank.neese@cec.mpg.de.
*E-mail: jrlong@berkeley.edu.
*E-mail: chrischang@berkeley.edu.

Author Contributions

§These authors contributed equally.

Notes

The authors declare no competing financial interest.

■ ACKNOWLEDGMENTS

The synthesis, characterization, and reactivity studies described were supported by DOE/LBNL Grant 403801 (to C.J.C.). The contributions of J.R.L. were supported by NSF Grant CHE-1111900. C.J.C. is an Investigator with the Howard Hughes Medical Institute. The authors thank Prof. Karl Wieghardt and Dr. Thomas Weihermüller (Max-Planck Institute für Chemische Energiekonversion, Mülheim an der Ruhr, Germany) for helpful discussions.

■ DEDICATION

This paper is dedicated to Harry B. Gray.

■ REFERENCES

(1) For general reviews, see: (a) Rehder, D. *Coord. Chem. Rev.* **1999**, *182*, 297−322. (b) Butler, A. *Coord. Chem. Rev.* **1999**, *187*, 17−35. (c) Ligtenbarg, A. G. J.; Hage, R.; Feringa, B. L. *Coord. Chem. Rev.* **2003**, *237*, 89−101. (d) Yudenfreund Kravitz, J.; Pecoraro, V. L. *Pure Appl. Chem.* **2005**, *77*, 1595−1605. For selected individual studies, see: (e) Colpas, G. J.; Hamstra, B. J.; Kampf, J. W.; Pecoraro, V. L. *J. Am. Chem. Soc.* **1994**, *116*, 3627−3828. (f) Colpas, G. J.; Hamstra, B. J.; Kampf, J. W.; Pecoraro, V. L. *J. Am. Chem. Soc.* **1996**, *118*, 3469−3478. (g) Messerschmidt, A.; Wever, R. *Proc. Nat. Acad. Sci. U.S.A.* **1996**, *93*, 392−396. (h) Kimblin, C.; Bu, X.; Butler, A. *Inorg. Chem.* **2002**, *41*, 161−163. (i) Groysman, S.; Goldberg, I.; Goldschmidt, Z.; Kol, M. *Inorg. Chem.* **2005**, *44*, 5073−5080. (j) Nica, S.; Pohlmann, A.; Plass, W. *Eur. J. Inorg. Chem.* **2005**, 2032−2036. (k) Zampella, G.; Fantucci, P.; Pecoraro, V. L.; De Gioia, L. *J. Am. Chem. Soc.* **2005**, *127*, 953−960. (l) Zampella, G.; Fantucci, P.; Pecoraro, V. L.; De Gioia, L. *Inorg. Chem.* **2006**, *45*, 7133−7143. (m) Mba, M.; Pontini, M.; Lovat, S.; Zonta, C.; Bernardinelli, G.; Kundig, P. E.; Licini, G. *Inorg. Chem.* **2008**, *47*, 8616−8618.

(2) (a) Itoh, T.; Jitsukawa, K.; Kaneda, K.; Teranishi, S. *J. Am. Chem. Soc.* **1979**, *101*, 159−69. (b) Chang, C. J.; Labinger, J. A.; Gray, H. B. *Inorg. Chem.* **1997**, *36*, 5927−5930. (c) Smith, K. I.; Borer, L. L.; Olmstead, M. M. *Inorg. Chem.* **2003**, *42*, 7410−7415.

(3) (a) Hirao, T.; Mori, M.; Ohshiro, Y. *J. Org. Chem.* **1990**, *55*, 358−360. (b) Moriuchi, T.; Kikushima, K.; Kajikawa, T.; Hirao, T. *Tetrahedron Lett.* **2009**, *50*, 7385−7387.

(4) (a) Rocek, J.; Aylward, D. E. *J. Am. Chem. Soc.* **1975**, *97*, 5452−5456. (b) Maeda, Y.; Kakiuchi, N.; Matsumura, S.; Nishimura, T.; Kawamura, T.; Uemura, S. *J. Org. Chem.* **2002**, *67*, 6718−6724. (c) Velusamy, S.; Punniyamurthy, T. *Org. Lett.* **2004**, *6*, 217−219.

(d) Hanson, S. K.; Baker, R. T.; Gordon, J. C.; Scott, B. L.; Silks, L. A. P.; Thorn, D. L. *J. Am. Chem. Soc.* **2010**, *132*, 17804−17816. (e) Hanson, S. K.; Wu, R.; Silks, L. A. P. *Org. Lett.* **2011**, *13*, 1908−1911.
(5) (a) Hanson, S. K.; Baker, R. T.; Gordon, J. C.; Scott, B. L.; Sutton, A. D.; Thorn, D. L. *J. Am. Chem. Soc.* **2009**, *131*, 428−429. (b) Hanson, S. K.; Wu, R.; Silks, L. A. P. *Angew. Chem., Int. Ed.* **2012**, *51*, 3410−3413. (c) Zhang, G.; Scott, B. L.; Wu, R.; Silks, L. A. P.; Hanson, S. K. *Inorg. Chem.* **2012**, *51*, 7354−7361.
(6) Barhate, N. B.; Chen, C.-T. *Org. Lett.* **2002**, *4*, 2529−2532.
(7) Radosevich, A. T.; Musich, C.; Toste, F. D. *J. Am. Chem. Soc.* **2005**, *127*, 1090−1091.
(8) (a) Blanc, A.; Toste, F. D. *Angew. Chem., Int. Ed.* **2006**, *45*, 2096−2099. (b) Wuyts, S.; Wahlen, J.; Jacobs, P. A.; De Vos, D. E. *Green Chem.* **2007**, *9*, 1104−1108. (c) Radosevich, A. T.; Chan, V. S.; Shih, H.-W.; Toste, F. D. *Angew. Chem., Int. Ed.* **2008**, *47*, 3755−3758. (d) Chen, C.-T.; Kao, J.-Q.; Salunke, S. B.; Lin, Y.-H. *Org. Lett.* **2011**, *13*, 26−29.
(9) Son, S.; Toste, F. D. *Angew. Chem., Int. Ed.* **2010**, *49*, 3791−3794.
(10) (a) Tsuchida, E.; Yamamoto, K.; Oyaizu, K.; Iwasaki, N.; Anson, F. C. *Inorg. Chem.* **1994**, *33*, 1056−63. (b) Tsuchida, E.; Oyaizu, K.; Dewi, E. L.; Imai, T.; Anson, F. C. *Inorg. Chem.* **1999**, *38*, 3704−3708. (c) Liu, Z.; Anson, F. C. *Inorg. Chem.* **2000**, *39*, 274−280.
(11) Ballhausen, C. J.; Gray, H. B. *Inorg. Chem.* **1962**, *1*, 111−122.
(12) (a) Karunadasa, H. I.; Chang, C. J.; Long, J. R. *Nature* **2010**, *464*, 1329−1333. (b) Sun, Y.; Bigi, J. P.; Piro, N. A.; Tang, M. L.; Long, J. R.; Chang, C. J. *J. Am. Chem. Soc.* **2011**, *133*, 9212−9215. (c) Karunadasa, H. I.; Montalvo, E.; Sun, Y.; Majda, M.; Long, J. R.; Chang, C. J. *Science* **2012**, *335*, 698−702. (d) Sundstrom, E. J.; Yang, X.; Thoi, V. S.; Karunadasa, H. I.; Chang, C. J.; Long, J. R.; Head-Gordon, M. *J. Am. Chem. Soc.* **2012**, *134*, 5233−5242. (e) Thoi, V. S.; Karunadasa, H. I.; Surendranath, Y.; Long, J. R.; Chang, C. J. *Energy Environ. Sci.* **2012**, *5*, 7762−7770. (f) King, A. E.; Surendranath, Y.; Piro, N. A.; Bigi, J. P.; Long, J. R.; Chang, C. J. *Chem. Sci.* **2013**, *4*, 1578−1587. (g) Nippe, M.; Khnayzer, R. S.; Panetier, J. A.; Zee, D. Z.; Olaiya, B. S.; Head-Gordon, M.; Chang, C. J.; Castellano, F. N.; Long, J. R. *Chem. Sci.* **2013**, *4*, 3934−3945. (h) Sun, Y.; Sun, J.; Long, J. R.; Yang, P.; Chang, C. J. *Chem. Sci.* **2013**, *4*, 118−124.
(13) (a) Kashif, M. K.; Axelson, J. C.; Duffy, N. W.; Forsyth, C. M.; Chang, C. J.; Long, J. R.; Spiccia, L.; Bach, U. *J. Am. Chem. Soc.* **2012**, *134*, 16646−16653. (b) Kashif, M. K.; Nippe, M.; Duffy, N. W.; Forsyth, C. M.; Chang, C. J.; Long, J. R.; Spiccia, L.; Bach, U. *Angew. Chem., Int. Ed.* **2013**, *52*, 5527−5531.
(14) Freedman, D. E.; Jenkins, D. M.; Long, J. R. *Chem. Commun.* **2009**, 4829−4831.
(15) A search of the CCSD revealed three monovanadium complexes with V−O bond lengths greater than 1.62 Å: (a) Molinaro, F. S.; Ibers, J. A. *Inorg. Chem.* **1976**, *15*, 2278−2283. (b) Crans, D. C.; Chen, H.; Anderson, O. P.; Miller, M. M. *J. Am. Chem. Soc.* **1993**, *115*, 6769−6776. (c) Crans, D. C.; Keramidas, A. D.; Mahroof-Tahir, M.; Anderson, O. P.; Miller, M. M. *Inorg. Chem.* **1996**, *35*, 3599−3606.
(16) (a) Micera, G.; Garribba, E. *J. Comput. Chem.* **2011**, *32*, 2822−2835. (b) Lodyga-Chruscinska, E.; Micera, G.; Garribba, E. *Inorg. Chem.* **2011**, *50*, 883−899.
(17) (a) Budge, J. R.; Gatehouse, B. M. K.; Nesbit, M. C.; West, B. O. *J. Chem. Soc., Chem. Commun.* **1981**, 370−371. (b) Groves, J. T.; Kruper, W. J.; Haushalter, R. C.; Butler, W. M. *Inorg. Chem.* **1982**, *21*, 1363−1368.
(18) (a) Collins, T. J.; Powell, R. D.; Slebodnick, C.; Uffelman, E. S. *J. Am. Chem. Soc.* **1990**, *112*, 899−901. (b) MacDonnell, F. M.; Fackler, N. L. P.; Stern, C.; O'Halloran, T. V. *J. Am. Chem. Soc.* **1994**, *116*, 7431−7432.
(19) For selected examples, see: (a) Buchler, J. W.; Dreher, C.; Lay, K. L.; Lee, Y. J.; Scheidt, R. W. *Inorg. Chem.* **1983**, *22*, 888−891. (b) Du Bois, J.; Hong, J.; Carreira, E. M.; Day, M. W. *J. Am. Chem. Soc.* **1996**, *118*, 915−916. (c) Du Bois, J.; Tomooka, C. S.; Hong, J.; Carreira, E. M.; Day, M. W. *Angew. Chem., Int. Ed.* **1997**, *36*, 1645−1647. (d) Chang, C. J.; Connick, W. B.; Low, D. W.; Day, M. W.; Gray, H. B. *Inorg. Chem.* **1998**, *37*, 3107−3110. (e) Meyer, K.; Bendix, J.; Metzler-Nolte, N.; Weyhermüller, T.; Wieghardt, K. *J. Am. Chem. Soc.* **1998**, *120*, 7260−7270. (f) Grapperhaus, C. A.; Bill, E.; Weyhermüller, T.; Nesse, F.; Wieghardt, K. *Inorg. Chem.* **2001**, *40*, 4191−4198.
(20) Berry, J. F.; Bill, E.; Bothe, E.; DeBeer George, S.; Mienert, B.; Neese, F.; Wieghardt, K. *Science* **2006**, *312*, 1937−1941.
(21) Waidmann, C. R.; Di Pasquale, A. G.; Mayer, J. M. *Inorg. Chem.* **2010**, *49*, 2383−2391.
(22) Bechlars, B.; D'Alessandro, D. M.; Jenkins, D. J.; Iavarone, A. T.; Glover, S. D.; Kubiak, C. P.; Long, J. R. *Nat. Chem.* **2010**, *2*, 362−368.
(23) *APEX2 v2009*; Bruker Analytical X-Ray Systems, Inc.: Madison, WI, 2009.
(24) Sheldrick, G. M. *SADABS*, version 2.03; Bruker Analytical X-ray Systems, Inc.: Madison, WI, 2000.
(25) Dolomanov, O. V.; Bourhis, L. J.; Gildea, R. J.; Howard, J. A. K.; Puschmann, H. *J. Appl. Crystallogr.* **2009**, *42*, 339−341.
(26) (a) Neese, F. *WIREs Comput. Mol. Sci.* **2012**, *2*, 73−78. (b) Neese, F. with contributions from Becker, U.; Ganyushin, G.; Hansen, A.; Izsak, R.; Liakos, D. G.; Kollmar, C.; Kossmann, S.; Pantazis, D. A.; Petrenko, T.; Reimann, C.; Riplinger, C.; Roemelt, M.; Sandhöfer, B.; Schapiro, I.; Sivalingam, K.; Wennmohs, F.; Wezisla, B. and contributions from our collaborators: Kállay, M.; Grimme, S.; Valeev, E. *ORCA—An ab initio, DFT and semiempirical SCF-MO package*, version 2.9.1; Max-Planck Institut für Chemische Energiekonversion: Mülheim an der Ruhr, Germany. The binaries of ORCA are available free of charge for academic users for a variety of platforms.
(27) Neese, F.; Wennmohs, F.; Hansen, A.; Becker, U. *Chem. Phys.* **2009**, *356*, 98−109.
(28) Neese, F. *J. Comput. Chem.* **2003**, *24*, 1740−1747.
(29) Malmqvist, P.-Å; Roos, B. O. *Chem. Phys. Lett.* **1989**, *155*, 189−194.
(30) (a) Angeli, C.; Cimiraglia, R.; Malrieu, J.-P. *Chem. Phys. Lett.* **2001**, *350*, 297−305. (b) Angeli, C.; Cimiraglia, R.; Evangelisti, S.; Leininger, T.; Malrieu, J.-P. *J. Chem. Phys.* **2001**, *114*, 10252−10264. (c) Angeli, C.; Cimiraglia, R.; Malrieu, J.-P. *J. Chem. Phys.* **2002**, *117*, 9138−9153. (d) Borini, S.; Cestari, M.; Cimiraglia, R. J. *J. Chem. Phys.* **2004**, *121*, 4043−4049. (e) Angeli, C.; Bories, B.; Cavallini, A.; Cimiraglia, R. *J. Chem. Phys.* **2006**, *124*, 054108-1−054108-8.
(31) (a) Jørgensen, C. K.; Pappalardo, R.; Schmidtke, H.-H. *J. Chem. Phys.* **1963**, *39*, 1422−1430. (b) Schäffer, C. E.; Jørgensen, C. K. *Mol. Phys.* **1965**, *9*, 401−412.
(32) (a) Atanasov, M.; Ganyushin, D.; Sivalingam, K.; Neese, F. *Struct. Bonding (Berlin)* **2012**, *143*, 149−220. (b) Atanasov, M. A.; Zadrozny, J. M.; Long, J. R.; Neese, F. *Chem. Sci.* **2013**, *4*, 139−156.